AIAA JOURNAL
Vol. 39, No. 9, September 2001

Structure of Supersonic Flames Imaged Using OH/Acetone Planar Laser-Induced Fluorescence

Rodney A. Bryant* and James F. Driscoll†
University of Michigan, Ann Arbor, Michigan 48109-2118

The general structure of a supersonic flame was identified by obtaining images of the laser-induced fluorescence from hydroxyl (OH) radicals and from acetone, which was used to mark the hydrogen fuel in the low-temperature region upstream of the lifted flame base. Results are compared to the numerical simulations of Roy and Edwards (Roy, C. J., and Edwards, J. R., "Numerical Simulation of a Three-Dimensional Flame/Shock Wave Interaction," *AIAA Journal*, Vol. 38, No. 5, 2000, pp. 745–754). The flame properties are significantly affected by the liftoff of the flame base and by the intense fuel/air mixing in the liftoff region, both of which are driven by the supersonic coflow. The lifted supersonic flame has the following two features that are associated with premixed flames: 1) there is significant mixing of air into the fuel stream upstream of the flame base (as evidenced by the rapid decrease in the fuel marker intensity in the low temperature liftoff region); 2) OH radicals (but not fuel) exist on the centerline everywhere downstream of the flame base. This condition is significantly different from the conditions within attached jet flames, which typically contain fuel near the centerline from the flame base to the flame tip. The results indicate that precautions should be taken in the attempt to model lifted flames, so that the premixed nature of the flame base is simulated correctly.

Nomenclature

d = inner diameter of fuel injector tube, 0.70 cm
I = fluorescence intensity
M_c = convective Mach number
n = gas number density
r = radial coordinate
S_f^* = sensitivity factor of acetone fluorescence
T = gas temperature
x = axial coordinate

Subscripts

AC = acetone fuel marker
H2 = hydrogen fuel
0 = condition at exit of fuel injector tube

Introduction

ONE motivation for studying the structure of supersonic flames is that it is not practical to test scramjet combustors over the entire range of expected conditions. Therefore, it is necessary to rely on computational models, such as those developed by Roy and Edwards,[1] Ecklund et al.,[2] Villasenor et al.,[3] Baurle et al.,[4] and Zheng and Bray.[5] Unfortunately, little is known about the reaction zone structure within supersonic flames, and so the models must rely on assumptions that have not been experimentally verified. For example, certain models assume that if the fuel and the air enter the supersonic combustor in separate streams, a two-stream conserved scalar approach can be used that does not allow for any premixing of the fuel and air except in a region very close to the reaction zone. Such models also do not allow the flame to propagate at its own propagation speed, as would a premixed flame.

To assess such assumptions, it is useful to image the structure of a supersonic flame that has a simple geometry. The goal of the present work was to determine the general shape (and location) of the fuel zone and the OH radical zone in a supersonic flame. The results are compared to some recent simulations of Roy and Edwards,[1] who computed the OH and fuel concentrations for the same geometry and run conditions as the present experiment. Previously, several other quantities have been measured in this combustor, including flame lengths,[6] blowout limits,[7] pressure distributions,[8] shock wave structure,[9] and combustion efficiencies.[10]

An important factor that affects the flame structure is the degree of liftoff of the flame base because intense fuel/air mixing can occur in the liftoff region. Supersonic flames are normally lifted because some type of bluff body (such as a rear-facing step or strut) normally is used to produce a low-speed wake in which the flame stabilizes. Some examples of lifted supersonic flames were reported by Cheng et al.,[11] Barlow et al.,[12] Ortwerth et al.,[13] and Guerra et al.,[14] and also include the flames studied in our laboratory.[6–10] Liftoff also occurs in supersonic flames that are stabilized in a crossflow, as reported by Hasselbrink and Mungal,[15] Segal et al.,[16] and Sabelnikov et al.[17] Some images of reaction zones in supersonic reacting shear layers were reported by Miller et al.,[18] Barlow et al.,[12] and Abbitt et al.[19]

Experimental Arrangement

Figure 1 shows a schematic of the experiment and a direct photograph of the supersonic flame. The facility is described in more detail by Driscoll et al.[6] and Yoon et al.[7,8] Air is expanded to Mach 2.5 through a two-dimensional converging–diverging nozzle that was designed using the method of characteristics. The combustor section was designed to diverge to eliminate thermal choking because thermal choking occurred in all cases when a constant area combustor section was used. Two of the combustor sidewalls are parallel for optical access whereas the other two sidewalls diverge at a half-angle of 4 deg. The combustor width is 5.8 cm at the fuel injection plane; the width is 11.1 cm at the exit of the combustor. The 55.3-cm-long diverging section is followed by a 50.0-cm-long constant area section that is 11.1 cm in width. All components are stainless steel, and the three windows in the combustor are fused silica. The trapezoidal front window has a height of 30.4 cm; its width is 6.6 cm at the bottom and 10.9 cm at the top. The two side windows are 1 cm wide and 30.4 cm high. The diffuser wall is water cooled. The uniformity of the flow in the supersonic test section was measured using pitot and wall pressure probes, as reported by Yoon et al.[8]

The bluff-body fuel injector is stainless steel tube having an outside diameter of 2.54 cm; fuel flows through a central tube that has an inside diameter d of 0.70 cm. Hydrogen is injected at a sonic velocity of 1191 m/s. The Mach number of the air at the injector plane

Received 20 March 1999; revision received 11 January 2001; accepted for publication 6 February 2001.

*Research Assistant, Department of Aerospace Engineering; currently Mechanical Engineer, Mail Stop 8653, National Institute of Standards and Technology, 100 Bureau Drive, Gaithersburg, MD 20899; rbryant@nist.gov. Member AIAA.

†Professor, Department of Aerospace Engineering; jamesfd@umich.edu. Associate Fellow AIAA.

Table 1 Flow conditions for the three flames studied

Parameter	Supersonic flame A	Supersonic flame B	Subsonic flame C with coflow air
Fuel flow rate, g/s	0.95	1.4	0.83
Airflow rate, kg/s	1.09	1.09	0.2
Air velocity, m/s	564	564	92.7
Air Mach number	2.5	2.5	0.27
Fuel velocity, m/s	1,105	1,087	224
Fuel Mach number	1.0	1.0	0.18
Fuel Reynolds number	81,000	82,000	16,000
Air stagnation temperature, K	285	285	289
Air stagnation pressure, atm	6.44	6.44	1.2
Acetone mole fraction	0.0058	0.0072	0.0053

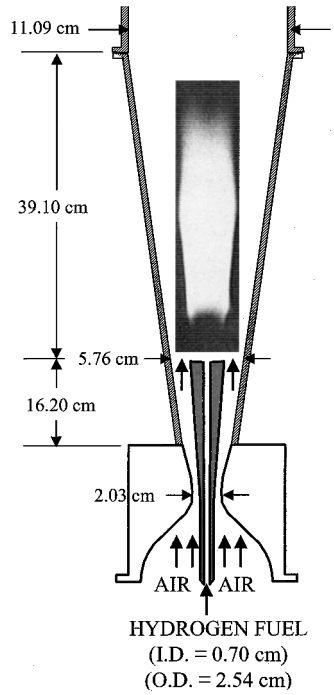

Fig. 1 Schematic diagram of the University of Michigan supersonic flame facility, including a direct photograph of the flame luminosity.

is 2.5 and is uniform to within 10%, as determined from pitot and static pressure measurements. The Mach number decreases by 30% along the length of the test section.[8] The fuel tube has a length of 94d, so that the fuel velocity profile can be assumed to correspond to that of fully developed turbulent pipe flow. Fuel and air mass flow rates are monitored using calibrated choked orifices. Table 1 lists the values of the fuel and air properties. The two supersonic flames that were imaged correspond to fuel flow rates of 0.95 and 1.4 g/s, respectively.

Trace amounts of acetone were added to the hydrogen to achieve an acetone mole fraction of 0.0072. A fraction of the hydrogen flow was bubbled through liquid acetone. It was verified that the acetone mole fraction in this stream of hydrogen was approximately the known saturation mole fraction because the acetone mole fraction [as monitored by the planar laser-induced fluorescence (PLIF) system] did not change with the residence time of the gas in the acetone chamber. This stream of saturated gas was mixed with the remaining pure hydrogen to achieve the desired mole fraction of acetone. The use of acetone as a flow tracer is described by Lozano et al.,[20] Thurber et al.,[21,22] Thurber and Hanson,[23] Grossmann et al.,[24] Bryant et al.,[25] and Glawe et al.[26]

The acetone fluorescence was excited using the quadrupled output of a Spectra-Physics GCR-250 Nd-YAG laser at a wavelength of 266 nm. Fluorescence was detected at wavelengths between 330 and 550 nm; the BK7 glass lenses effectively blocked the laser light at 266 nm so that no optical filters were needed. Images of the OH concentration field were obtained by doubling the output of a Lumonics HD-500 Nd:YAG-pumped dye laser to 282.75 nm to excite the $Q_1(5)$ line of the (1, 0) band of the $A^2\Sigma \leftarrow X^2\Pi$ transition of the OH molecule. OH fluorescence was collected in the wavelength range from 295 to 480 nm using a combination of two Schott glass filters (SWG 295 and a SBG-1) and a UV Nikor lens. A cooled, slow-scan, intensified charge-coupled device (ICCD) array camera (Princeton Instruments ICCD 576) was used to image a field of view of 7.6 × 5.1 cm; the laser light sheet thickness was 300 mm. Calibration measurements indicated that the fluorescence was not in the saturated regime but was a linear function of the laser intensity. The laser pulse duration was 10 ns, and the fluorescence was collected during the 180-ns gated exposure time of the ICCD camera. There was no interference between the acetone and OH PLIF signals because they were measured during different runs.

A correction was made to remove spatial variations in the intensity of the laser sheet; each image was normalized by an image of acetone vapor that was uniformly distributed in space. Shot-to-shot variations in the laser energy/pulse were measured to be 10%, and each image was normalized by the measured laser energy. The measured background light due to window fluorescence was measured to be 4% of the signal and was subtracted. In addition, the shot noise was reduced by applying a spatial filter that assigns the median of a 3 × 3 pixel region to the central pixel.

Results

PLIF Images of the Structure of a Lifted Supersonic Flame

Figure 2a is a composite of instantaneous images of the fluorescence from OH and the acetone fuel marker in the lifted supersonic flame for a fuel mass flow rate of 0.95 g/s. For comparison, Fig. 2b is a composite of images of a subsonic hydrogen/air flame that was operated with a fuel flow rate (0.83 g/s) that is similar to that of the supersonic flame. The coflow air velocity of the subsonic flame is 92.7 m/s. To obtain Fig. 2a, the entire flame could not be imaged at one instant; instead, the flame zone was divided up into five regions and instantaneous PLIF images of each region were recorded at random times. Test conditions are listed in Table 1.

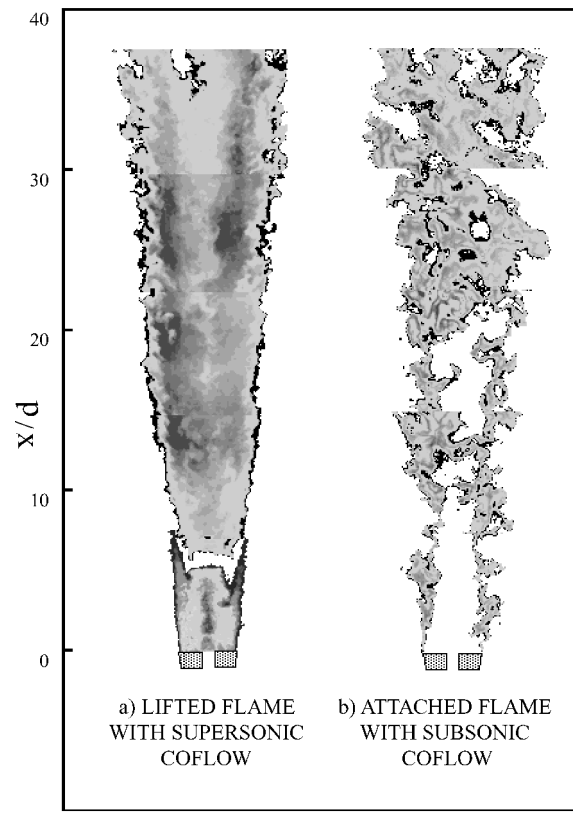

Fig. 2 Instantaneous images of the OH fluorescence intensity in a) the lifted supersonic flame and b) an attached subsonic flame, with coflow air velocity of 92.7 m/s; fuel is hydrogen, d is the fuel injector i.d. = 0.7 cm; also shown is the fluorescence intensity of the acetone fuel marker in the supersonic case.

There are two major differences between the lifted flame and the attached flame shown in Fig. 2.

1) In the lifted flame (Fig. 2a) there is evidence of significant premixing of fuel and air before combustion. When such fuel/air premixing occurs, the combustion can no longer be considered to be nonpremixed.

2) In the attached flame (Fig. 2b) there is a continuous OH layer that separates the fuel and the air, which is a characteristic of a nonpremixed flame. However, in the lifted flame there is no OH layer separating fuel and air; instead OH is observed everywhere downstream of the reaction zone, which is characteristic of premixed combustion.

Evidence that fuel/air mixing occurs (before combustion) in the flame shown in Fig. 2a is the observation that the normalized acetone fuel marker fluorescence decreases rapidly along the centerline in the relatively low-temperature liftoff region upstream of the flame base. This fuel marker intensity decreases from a value of 1.0 at $x = 0$ to 0.1 at $x/d = 7$. In the next section, analysis is provided that indicates that most of the decrease in fuel marker along the centerline is due to fuel/air mixing, and no more than approximately 20% of the decrease can be attributed to possible differential diffusion and acetone decomposition.

Figure 2b shows that in the attached flame the OH layers surround a white region that exists near the centerline from $x/d = 0$ to 20. Because this enclosed white region is directly above the fuel injector, it is believed that the white region contains fuel and products. The OH layers are seen to form a boundary between this centerline region and the surrounding air. Barlow et al.[27] have shown that in an attached nonpremixed flame, the probability that oxygen can penetrate through the OH reaction zone is small; a typical oxygen concentration on the fuel side of their flame is less than 1%. The two fundamental differences between nonpremixed and premixed flames are that premixed flames have air that is premixed with the fuel and have a continuous region of OH downstream, whereas nonpremixed flames typically have no air premixed with the fuel and have OH layers between the fuel and the air.

Several other differences between the lifted and attached flames that are observed, and that can be explained by the degree of premixing, include 1) the shapes of the OH radical region and the OH profiles, 2) the shape of the fuel concentration profiles, 3) the shape of the flame tip, and 4) the presence of OH layers and pockets of entrained gas.

The OH region in the lifted flame (Fig. 2a) is seen to have a relatively uniform concentration of radicals, whereas the OH region in the attached flame consists of entangled OH layers that surround pockets that are devoid of OH. It is not known if these pockets contain fuel or air. In the lifted flame, the OH exists on the centerline at a relatively small value of $x/d = 7$, whereas in the attached flame the OH does not consistently appear on centerline until x/d exceeds 20. Seitzman et al.[28] have reported OH images in jet flames, and they also did not observe OH on centerline upstream of $x/d = 20$.

Another observation is that the tip of the lifted supersonic flame in Fig. 2a is not pointed but has a V-shaped OH pattern near the tip. This V-shaped pattern has been observed in the rod-stabilized premixed flames that were studied by Cheng.[29] An attached nonpremixed flame has a pointed tip because the mean radial location of the stoichiometric contour (and the chemical reaction zone) must approach zero at the tip as all of the fuel is consumed. However, if liftoff occurs and premixing occurs upstream of the flame base, there is no requirement that the reaction zone approach the centerline near the tip. Although the tip region in Fig. 2a has a V shape that is similar to the premixed flame of Cheng, the two experiments differ in several ways, so that a quantitative comparison cannot be made.

One feature of the supersonic flame in Fig. 2a is that the OH boundary is relatively smooth and has no large-scale wrinkles, whereas the OH boundary of the subsonic flame in Fig. 2b has large wrinkles. The large wrinkles in the subsonic case are an indicator of large-scale engulfment of air. There are several possible reasons why large-scale wrinkles and large-scale engulfment are not observed in the supersonic case. The jet Reynolds number of 7.6×10^4 may be so large that fine-grained turbulence dominates the mixing process.

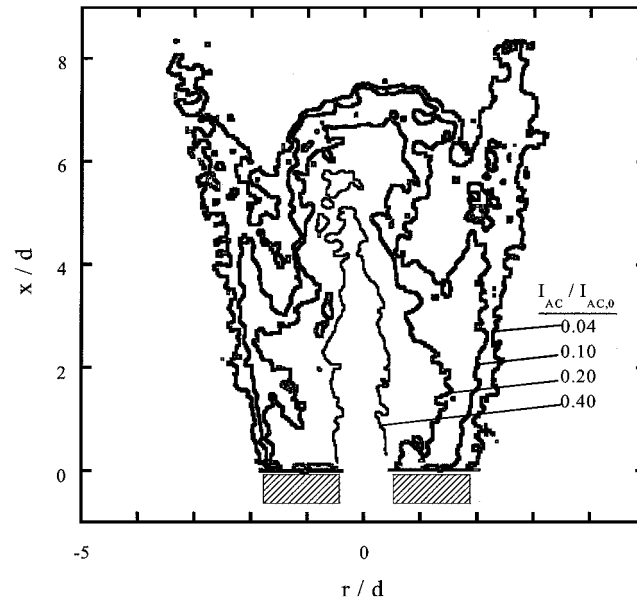

Fig. 3 Magnified view of the instantaneous contours of the acetone fuel marker fluorescence in the supersonic flame.

Buoyancy forces are negligible in the supersonic case, and so the contribution of buoyancy to the creation of large eddies near the edge of the jet is negligible. Another possible reason is that eddies are rapidly convected across the flame due to the supersonic coflow velocity, and, therefore, eddies have insufficient residence time to roll up the flame and cause large wrinkles.

The fuel/air mixing in the supersonic flame can be better understood by closely examining the liftoff region, which is shown as contours in Fig. 3. The acetone fuel marker normalized intensity is between 1.0 and 0.4 in the short central core jet region on the centerline. The outer contour, where the normalized intensity is 0.04, shows that acetone is entrained into the outer shear layer. This contour outlines two peninsulas, created by the shear layer, which can extend downstream farther than the centerline acetone. There is evidence that recirculation behind the bluff-body fuel injector forces some fuel to move in the radial direction; acetone is observed at the location $x/d = 0$, $r/d = 2$, which is the outer corner of the fuel injector. Because all of the fuel initially exits the injector near the centerline region, recirculation is required to transport the fuel upstream to locations far from centerline at $x/d = 0$.

Interpretation of the Fluorescence Signal

The acetone fluorescence decays rapidly in the axial direction (Figs. 2a and 3), which can be due to three factors: the rapid mixing of air into the fuel, possible decomposition of acetone, and differential diffusion. The decomposition of acetone occurs as the acetone temperature approaches 1000 K (Refs. 21–23). A problem can arise in an attached jet flame because the hydrogen fuel could exist for several centimeters downstream of the location where the acetone has disappeared. However, this problem cannot arise in the present lifted flame because OH radicals exist immediately downstream of the location where acetone disappears ($x/d = 7$). The hydrogen fuel jet cannot penetrate into the OH region and remain unreacted because OH is a highly reactive oxidizer. Acetone decomposition most likely does occur within the premixed reaction zone at the flame base; for hydrogen and air this reaction zone is typically less than 1 mm in thickness. Thus, it is believed that the acetone fluorescence is an accurate marker of the fuel location in the lifted flame, except in the 1-mm region near the OH boundary.

In the liftoff region where the acetone fluorescence is measured, it can be argued that the gas temperature does not exceed 1000 K because OH fluorescence is a good marker of fluid elements that have a temperature above 1000 K, and OH is not observed in the liftoff region. The primary way in which fluid is heated to 1000 K is by turbulent or molecular diffusion of energy because OH diffuses

at approximately the same rate as energy. It is unlikely that differential diffusion effects are so large that gas temperature could exceed 1000 K in the liftoff region where there is no OH present. Radiative heating of the reactants is negligible in a hydrogen/air flame. Therefore, the axial decay of the acetone fluorescence in the liftoff region is not believed to be significantly affected by acetone decomposition.

Additional errors due to differential diffusion are estimated to be less than 6%, based on the measurements of Smith et al.[30] They defined the error that arises because different species diffuse at different rates to be the standard deviation of the difference between ζ_H and ζ_C , which are conserved scalars based on the mass fraction of hydrogen atoms and carbon atoms, respectively. Their measurements showed that the differential diffusion error decreases from 8% at a jet Reynolds number of 8×10^3 to 7% at $Re = 1.6 \times 10^4$ to 6% at $Re = 3 \times 10^4$. The value for the present experiment is $Re = 7.6 \times 10^4$, and so the differential diffusion error is estimated to be less than 6%.

It was not possible to determine quantitative values of the fuel number density from the acetone PLIF images shown in Figs. 2a and 3 because such an analysis requires that the gas temperature be measured. Temperatures were not measured using physical probes that would disturb the sensitive recirculation zone. However, it is possible to estimate the fuel number density if two assumptions are made.

The intensity of the fluorescence from the acetone tracer that was added to the fuel I_{AC} is related to the number density of acetone n_{AC} by the following relation:

$$(I_{AC}/I_{AC,0}) = (n_{AC}/n_{AC,0}) \cdot S_f^*(\lambda, T) \tag{1}$$

which was discussed by Thurber et al.[21,22] and Thurber and Hanson.[23] The subscript 0 denotes conditions at the exit of the fuel injector. Thurber et al. also report that the sensitivity factor S_f^* for a laser wavelength of 266 nm is given by

$$S_f^* = 0.90 + 0.25(T/300\,\mathrm{K}) - 0.15(T/300\,\mathrm{K})^2 \tag{2}$$

Equation (2) shows that acetone is not an acceptable fuel tracer at gas temperatures exceeding 1000 K because S_f^* decreases to 0.07 at 1000 K. However, over the temperature range from 300 to 600 K the value of S_f^* in Eq. (2) deviates from unity by less than 20%. In Fig. 2a it is seen that the acetone fuel tracer exists only upstream of the lifted flame base. Although the temperature in this liftoff region is not known, the numerical simulation of the present flame by Roy and Edwards[1] shows good agreement with the present results (as described in the next section); the simulation predicts that nearly all of the liftoff region has a temperature below 600 K. This is expected because Fig. 3 shows that there is mixing between the cold fuel and the cold air in the liftoff region.

An estimate of the fuel number density in the liftoff region can be made if two assumptions are made, that the gas temperature in the liftoff region does not exceed 600 K and that differential diffusion effects are negligible. If these assumptions are valid, one can conclude, with a 20% uncertainty, that

$$(n_{H2}/n_{H2,0}) = (I_{AC}/I_{AC,0}) \tag{3}$$

where $n_{H2,0}$ is 2.2×10^{19} cm^{-3}.

Some Comparisons to Numerical Simulations of Roy and Edwards[1]

Figure 4a shows the contours of the OH and the acetone intensities that were obtained by averaging 100 PLIF images. For comparison, the computed mean profiles reported by Roy and Edwards[1] are displayed in Fig. 4b. In their simulation, Roy and Edwards considered a fuel injector geometry and a wind-tunnel side wall geometry that were identical to that of the present experiment. Their computational domain was rectangular to match that of the wind-tunnel combusting region. They also matched their inlet conditions and mass flow rates to the present experiment. It is seen that the base of the computed flame, defined as the band of maximum OH ($Y_{OH} = 0.009$) and maximum temperature, is lifted to an x/d location of 6. This is in agreement with the present experiment. The computed contours of fuel mass fraction decrease rapidly from 1.0 to 0.2 in the short distance upstream of x/d of 6, which is also in general agreement with the experiment. The decrease of the fuel mass fraction along

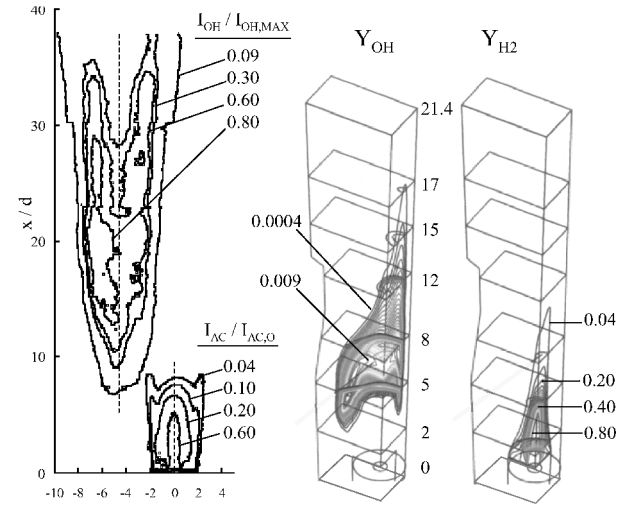

Fig. 4 Qualitative comparison of the experimental results to the computations of Roy and Edwards.[1] (Measurements in panel a are the average of 100 images.) The OH contours are shifted to the left for clarity due to the overlap with the acetone contours in the axial direction. Computations of mass fraction of OH and hydrogen are displayed in panel b. (Figure 4b originally published in "Numerical Simulation of a Three-Dimensional Flame/Shock Wave Interaction," Roy, C. J., and Edwards, J. R., *AIAA Journal*, Vol. 38, No. 5, 2000, pp. 745–754. Copyright © 2000 by the American Institute of Aeronautics and Astronautics, Inc. Reprinted with permission.)

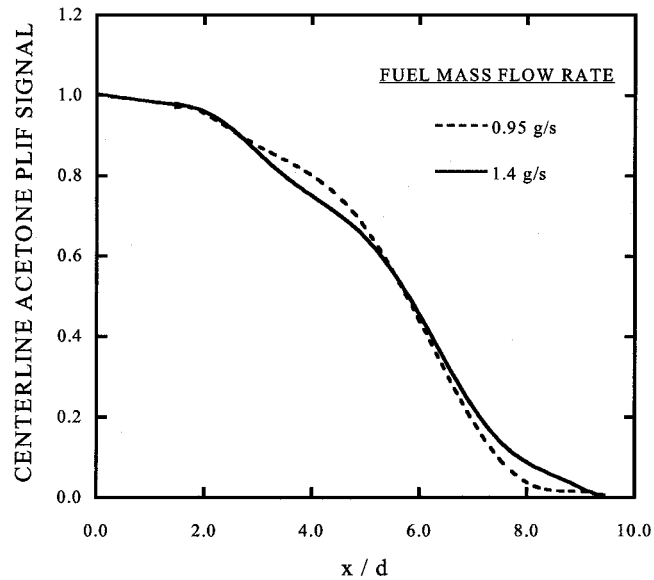

Fig. 5 Axial profiles of the mean fluorescence intensity of the acetone fuel marker on the centerline in two supersonic flames; conditions are listed in Table 1.

the centerline is entirely due to rapid fuel/air mixing in the simulation, and the computed gas temperatures in the liftoff zone are less than 600 K.

One difference between the measurements and the simulation is that peninsulas of fuel extend downstream in the shear layer in Fig. 3, but they are not seen in the computations of Roy and Edwards.[1] Another difference is that the simulation underpredicts the length of the OH reaction zone. However, a quantitative comparison of OH mass fractions cannot be made; measurements of species concentrations and gas temperatures that are required to determine the OH collisional quenching rate are not available.

Axial and Radial Profiles of Supersonic Flame Properties

Figures 5 and 6 quantify the variation of the mean acetone and OH fluorescence intensities along the centerline of the supersonic

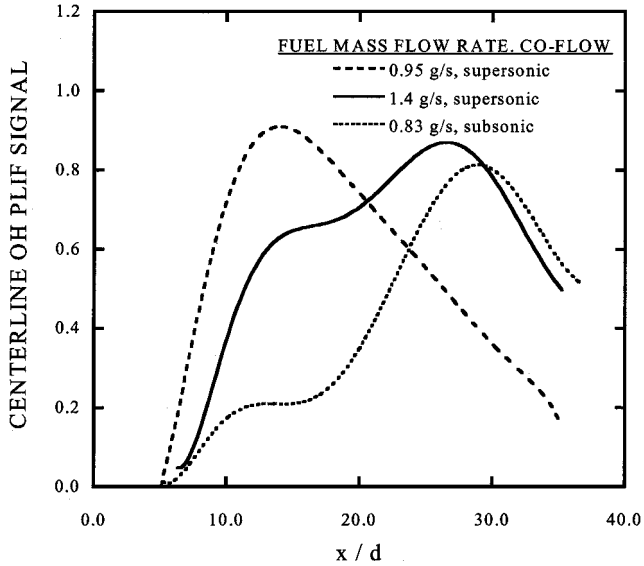

Fig. 6 Axial profiles of the OH mean fluorescence intensity on the centerline in two supersonic flames and the subsonic flame with coflow air.

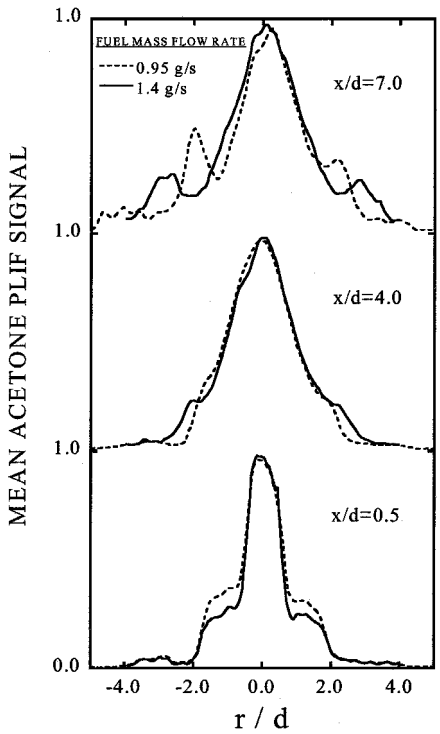

Fig. 7 Radial profiles of the mean fluorescence intensity of the acetone fuel marker in two supersonic flames; profiles are normalized by the local maximum.

flames. Averages were determined from 100 instantaneous images; run conditions are listed in Table 1. Figure 5 shows that the acetone intensity has decayed from 1.0 to 0.2 in the region between $x/d = 0$ and 7. At $x/d = 7$ the OH signal begins to increase in Fig. 6, so that the mean position of the flame base is $x/d = 7$.

The OH intensities along the centerline of the two supersonic flames appear in Fig. 6. The OH signal increases rapidly at the flame base ($x/d = 7$) and then decreases downstream. This rapid rise in the OH signal is characteristic of a premixed flame.[29] Figure 6 shows that the OH signal in the subsonic flame gradually increases until it reaches a maximum at $x/d = 30$. A gradual increase in the OH signal along the centerline is characteristic of nonpremixed jet flames.[27]

Figures 7 and 8 show the radial profiles of the mean acetone and OH intensities in the supersonic flames. The profiles in Fig. 7

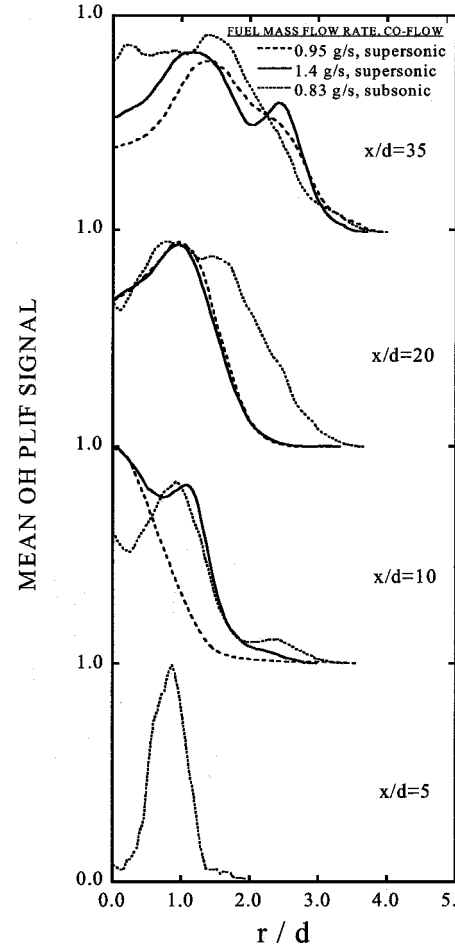

Fig. 8 Radial profiles of the mean OH fluorescence intensities within the two supersonic flames and the subsonic flame with coflow air; profiles are normalized by the local maximum.

differ from profiles measured in simple jets because of the presence of a recirculation zone and an outer shear layer. At $x/d = 0.5$ the acetone profile displays distinct steps, and at $x/d = 7$ there are three local maxima to the profile. Two of the local maxima are due to the peninsulas of acetone that are observed to be entrained into the shear layer in Figs. 2a and 3.

The radial profiles of OH intensity are shown in Fig. 8. It is seen that the OH intensities are relatively large on the centerline of the supersonic flames at all axial locations considered in Fig. 8, which indicates that unburned fuel is not present near the centerline at x/d locations exceeding 10. At downstream locations, $x/d = 20$ and 35, the OH signal of the supersonic flames reaches a maximum value at r/d locations of 1.0 and 1.4, respectively. The V-shaped appearance of the flame in the OH PLIF images is due to the presence of these local maxima in the OH signal.

By comparison of the profiles in Figs. 7 and 8, it is concluded that increasing the fuel flow rate causes a corresponding increase in the width of the OH and acetone profiles in the supersonic flame. This is consistent with the earlier finding that the length of the supersonic flame increases as the fuel flow rate is increased.[6] The flame width has practical importance; if the low-density OH region becomes sufficiently wide, the effective area of the supersonic coflow is reduced, and this blockage can promote thermal choking of the combustor.

Error Analysis and Effects of Compressibility

The 95% confidence interval[31] for each value of the mean OH and acetone fluorescence that is presented in Figs. 4a and 5–8 is the mean value reported plus or minus the margin of error, which is $1.96\sigma/N^{1/2}$. The number of images used to determine the average N was 100. The standard deviation of the fluorescence σ, which includes the variations due to turbulence and shot noise, was measured to have a typical value of 30% of the mean signal. Therefore, the

margin of error for the values in Figs. 4a and 5–8 is ±6% of the mean value. The uncertainty in the fuel flow rate is estimated to be 2%; this is the square root of the sum of the squares of the uncertainties of the choked orifice area (1%) and the stagnation pressure (1.5%). The uncertainty of the airflow rate is 2%. The uncertainty of the measured value of radial and axial position is 1%. The potential errors associated with differential diffusion and acetone decomposition were discussed earlier. The ability to resolve the fine-grained structure in the OH and acetone fluorescence images is limited by the spatial resolution, which is equal to the laser sheet thickness of 300 μm.

Compressibility effects were estimated by computing the convective Mach number M_c at the fuel injector ($x/d = 0$). Papamoschou and Roshko[32] showed that M_c is $(U_1 - U_c)/a_1$, where the convective velocity U_c is $(U_1 a_2 + U_2 a_1)/(a_1 + a_2)$. At the fuel injector the fuel velocity U_1 is 1191 m/s, the air velocity U_2 is 745 m/s, the speed of sound a_1 is 1191 m/s and a_2 is 299 m/s. M_c is 0.3 at the fuel injector, and it decreases in the downstream direction because the air Mach number remains constant but the velocity in the fuel jet decreases. Thus, M_c is less than 0.3 everywhere. Reference 33 indicates that for the present values of convective Mach number, the effects of compressibility on the mixing are negligible. In addition, Fig. 2 shows that the fuel/air mixing occurs in the subsonic region downstream of the fuel injector, and so compressibility effects on the present mixing process are believed to be negligible.

Conclusions

1) Images are obtained in a lifted supersonic hydrogen/air flame of the fluorescence intensities of the OH radical and the acetone fuel marker. The images show the relative locations, shapes, and sizes of the zones where OH and fuel are present.

2) Significant premixing of the fuel and the air occurs in the liftoff region ($x/d < 7$) because the normalized acetone fluorescence decays rapidly from 1.0 to 0.2 along the centerline in this region. The acetone exists only in the relatively cold liftoff zone upstream of the flame, and so the variation in acetone intensity is believed to be primarily due to fuel/air mixing and not due to differential diffusion or the decomposition of acetone.

3) Because there is evidence that air is premixed into the fuel prior to combustion, the base of the present flame is expected to have the nature of a premixed flame. Precautions should be taken in the modeling of such flames to account for a flame propagation speed and to avoid the assumption that the flame must be confined to the stoichiometric contour.

4) The OH reaction zone in the lifted supersonic flame is relatively homogeneous. Unlike the subsonic case, the supersonic flame has no pockets of gas that are devoid of OH and has no OH layers. The edge of the supersonic OH reaction zone is relatively smooth, with wrinkles that are much smaller in amplitude than the subsonic case. The subsonic flame consists of thin OH layers that are intensely wrinkled and tangled, forming gas pockets devoid of OH.

5) Some experimental results are compared to the computed profiles of OH and fuel mass fraction that were reported by Roy and Edwards[1] for a geometry identical to the present experiment. The qualitative agreement is encouraging, but the computation underpredicts the length of the OH radical zone.

Acknowledgments

This research was supported by Air Force Office of Scientific Research Contract DOD G-F49620-95-1-00115 (monitored by Julian Tishkoff), by NASA Graduate Student Research Program Award NGT-1-52136 (monitored by Glenn Diskin, NASA Langley Research Center), by the National Consortium for Graduate Degrees for Minorities in Engineering and Science, Inc., and by the University of Michigan Rackham School of Graduate Studies.

References

[1]Roy, C. J., and Edwards, J. R., "Numerical Simulation of a Three-Dimensional Flame/Shock Wave Interaction," *AIAA Journal*, Vol. 38, No. 5, 2000, pp. 745–754.

[2]Eklund, D. R., Drummond, J. P., and Hassan, H. A., "Calculation of Supersonic Turbulent Reacting Coaxial Jets," *AIAA Journal*, Vol. 28, No. 9, 1990, pp. 1633–1641.

[3]Villasenor, R., Chen, J.-Y., and Pitz, R.W., "Modeling Ideally Expanded Supersonic Turbulent Jet Flows with Nonpremixed H_2–Air Combustion," *AIAA Journal*, Vol. 30, No. 2, 1992, pp. 395–402.

[4]Baurle, R. A., Alexopoulos, G. A., and Hassan, H. A., "Assumed Joint Probability Density Function Approach for Supersonic Turbulent Combustion," *Journal of Propulsion and Power*, Vol. 10, No. 4, 1994, pp. 473–576.

[5]Zheng, L. L., and Bray, K. N. C., "Application of New Combustion and Turbulence Models to H_2–Air Nonpremixed Supersonic Combustion," *Combustion and Flame*, Vol. 99, No. 3, 1990, pp. 440–452.

[6]Driscoll, J. F., Huh, H., Yoon, Y., and Donbar, J. M., "Measured Lengths of Supersonic Hydrogen–Air Jet Flames—Compared to Subsonic Flame Lengths—and Analysis," *Combustion and Flame*, Vol. 107, No. 1, 1996, pp. 176–186.

[7]Yoon, Y., Donbar, J., and Driscoll, J. F., "Blowout Stability Limits of a Hydrogen Jet Flame in a Supersonic, Heated Coflow Air Stream," *Combustion Science and Technology*, Vol. 97, Nos. 1 and 2, 1994, pp. 137–156.

[8]Yoon, Y., Donbar, J., Huh, H., and Driscoll, J. F., "Measured Supersonic Flame Properties: Heat-Release Patterns, Pressure Losses, Thermal Choking Limits," *Journal of Propulsion and Power*, Vol. 12, No. 4, 1996, pp. 718–723.

[9]Huh, H., and Driscoll, J. F., "Shock-Wave Enhancement of the Mixing and the Stability Limits of Supersonic Hydrogen–Air Jet Flames," *26th Symposium (International) on Combustion*, Combustion Inst., Pittsburgh, PA, 1996, pp. 2933–2939.

[10]Ratner, A., Driscoll, J. F., Huh, H., and Bryant, R., "Combustion Efficiencies of Supersonic Flames," *Journal of Propulsion and Power*, Vol. 17, No. 2, 2001, pp. 301–307.

[11]Cheng, T. S., Wehrmeyer, J. A., Pitz, R. W., Jarrett, O., and Northam, G. B., "Raman Measurements of Mixing and Finite Rate Chemistry in a Supersonic Hydrogen–Air Diffusion Flame," *Combustion and Flame*, Vol. 99, No. 1, 1994, pp. 157–173.

[12]Barlow, R. S., Fourguette, D. C., Mungal, M. G., and Dibble, R. W., "Experiments on the Structure of an Annular Compressible Reacting Shear Layer," *AIAA Journal*, Vol. 30, No. 9, 1992, pp. 2244–2251.

[13]Ortwerth, P., Mathur, A., Vinogradov, V., and Grin, V., "Experimental and Numerical Investigation of Hydrogen and Ethylene Combustion in a Mach 3–5 Channel," AIAA Paper 96-3245, 1996.

[14]Guerra, R., Waidmann, W., and Laible, C., "Experimental Investigation of the Combustion of a Hydrogen Jet Injected Parallel in a Supersonic Airstream," AIAA Paper 91-5102, 1991.

[15]Hasselbrink, E. F., Jr., and Mungal, M. B., "Observations on the Stabilization Region of Lifted Nonpremixed Methane Transverse Jet Flames," *27th Symposium (International) on Combustion*, Combustion Inst., Pittsburgh, PA, 1998, pp. 1167–1173.

[16]Segal, C., McDaniel, J. C., Whitehurst, R. B., and Krauss, R. H., "Mixing and Chemical Kinetics Interactions in a Mach 2 Reacting Flow," *Journal of Propulsion and Power*, Vol. 11, No. 2, 1995, pp. 308–316.

[17]Sabelnikov, V. A., Voloschenko, O., Ostras, V., and Sermanov, V., "Gasdynamics of Hydrogen Fueled Scramjet Combustors," AIAA Paper 93-2145, 1993.

[18]Miller, M. F., Bowman, C. T., and Mungal, M. G., "An Experimental Investigation of the Effects of Compressibility on a Turbulent Reacting Mixing Layer," *Journal of Fluid Mechanics*, Vol. 356, No. 1, 1998, pp. 25–64.

[19]Abbit, J. D., Segal, C., McDaniel, J. C., Krauss, R. H., and Whitehurst, R. B., "Experimental Supersonic Hydrogen Combustion Employing Staged Injection Behind a Rearward-Facing Step," *Journal of Propulsion and Power*, Vol. 9, No. 3, 1993, pp. 472–478.

[20]Lozano, A., Yip, B., and Hanson, R. K., "Acetone: a Tracer for Concentration Measurements in Gaseous Flows by Planar Laser Induced Fluorescence," *Experiments in Fluids*, Vol. 13, No. 6, 1992, pp. 369–376.

[21]Thurber, M. C., Grisch, F., Kirby, B. J., Votsmeier, M., and Hanson, R. K., "Measurements and Modeling of Acetone Laser Induced Fluorescence with Implications for Temperature Imaging Diagnostics," *Applied Optics*, Vol. 37, No. 21, 1998, pp. 4963–4978.

[22]Thurber, M. C., Grisch, F., and Hanson, R. K., "Temperature Imaging with Single- and Dual-Wavelength Acetone Planar Laser-Induced Fluorescence," *Optics Letters*, Vol. 22, No. 4, 1997, pp. 251–253.

[23]Thurber, M. C., and Hanson, R. K., "Pressure and Composition Dependences of Acetone Laser-Induced Fluorescence with Excitation at 248, 266, and 308 nm," *Applied Physics B—Lasers*, Vol. 69, No. 3, 1999, pp. 229–240.

[24]Grossmann, F., Monkhouse, P. B., Ridder, M., Sick, V., and Wolfrum, J., "Temperature and Pressure Dependencies of the Laser-Induced Fluorescence of Gas-Phase Acetone and 3-Pentanone," *Applied Physics B–Lasers*, Vol. 62, No. 3, 1996, pp. 249–253.

[25]Bryant, R. A., Donbar, J. M., and Driscoll, J. F., "Acetone Laser Induced Fluorescence for Low Pressure/Low Temperature Flow Visualization," *Experiments in Fluids*, Vol. 28, No. 5, 2000, pp. 471–476.

[26]Glawe, D. D., Donbar, J. M., Nejad, A. S., Sekar, B., Chen, T. H., Samimy, M., and Driscoll, J. F., "Parallel Fuel Injection from the Base of an Extended Strut into Supersonic Flow," AIAA Paper 94–0711, 1994.

[27]Barlow, R. S., Fiechtner, G. J., Carter, C. D., and Chen, J. Y., "Experiments on the Scalar Structure of Turbulent CO/H2N2 Jet Flames," *Combustion and Flame*, Vol. 120, No. 4, 2000, pp. 549–569.

[28]Seitzman, J. M., Ungut, A., Paul, P. H., and Hanson, R. K., "Imaging and Characterization of OH Structures in a Turbulent Nonpremixed Flame," *23rd Symposium (International) on Combustion*, Combustion Inst., Pittsburgh, PA, 1990, pp. 637–644.

[29]Cheng, R. K., "Conditional Sampling of Turbulence Intensities and Reynolds Stress in Premixed Turbulent Flames," *Combustion Science and Technology*, Vol. 41, Nos. 1 and 2, 1984, pp. 109–142.

[30]Smith, L. L., Dibble, R. W., Talbot, L., Barlow, R. S., and Carter, C. D., "Laser Raman Scattering Measurements of Differential Molecular Diffusion in Turbulent Nonpremixed Jet Flames of H2/CO2 Fuel," *Combustion and Flame*, Vol. 100, Nos. 1 and 2, 1995, pp. 153–161.

[31]Crow, E. L., Davis., F. A., and Maxfield, M. W., *Statistics Manual*, Dover, New York, 1960.

[32]Papamoschou, C., and Roshko, A., "The Compressible Turbulent Shear Layer–An Experimental Study," *Journal of Fluid Mechanics*, Vol. 197, 1988, pp. 453–477.

[33]Elliott, G. S., and Samimy, M., "Compressibility Effects in Free Shear Layers," *Physics of Fluids A–Fluid Dynamics*, Vol. 2, No. 7, 1990, pp. 1231–1240.

J. C. Hermanson
Associate Editor